AGU PUBLICATIONS

Geophysical Research Letters

RESEARCH LETTER
10.1002/2015GL066122

Special Section:
First Results from the MAVEN Mission to Mars

Implications of MAVEN Mars near-wake measurements and models

J. G. Luhmann[1], Chuanfei Dong[2], Yingjuan Ma[3], S. M. Curry[1], D. Mitchell[1], J. Espley[4], J. Connerney[4], J. Halekas[5], D. A. Brain[6], B. M. Jakosky[6], and C. Mazelle[7,8]

[1]Space Sciences Laboratory, University of California, Berkeley, California, USA, [2]AOSS Department, University of Michigan, Ann Arbor, Michigan, USA, [3]Institute of Geophysics and Planetary Physics, UCLA, Los Angeles, California, USA, [4]NASA/Goddard Space Flight Center, Greenbelt, Maryland, USA, [5]Department of Physics and Astronomy, University of Iowa, Iowa City, Iowa, USA, [6]Laboratory for Atmospheric and Space Physics, University of Colorado Boulder, Boulder, Colorado, USA, [7]CNRS, IRAP, Toulouse, France, [8]University Paul Sabatier, Toulouse, France

Key Points:
- Mars' solar wind interaction is often viewed as an induced magnetosphere type
- MHD models of the interaction suggest much of its wake magnetic flux is instead rooted in Mars
- MAVEN measurements show some support for this alternate picture, at least at the present epoch

Correspondence to:
J. G. Luhmann,
jgluhman@ssl.berkeley.edu

Citation:
Luhmann, J. G., et al. (2015), Implications of MAVEN Mars near-wake measurements and models, *Geophys. Res. Lett.*, *42*, 9087–9094, doi:10.1002/2015GL066122.

Received 10 SEP 2015
Accepted 16 OCT 2015
Accepted article online 5 NOV 2015
Published online 11 NOV 2015

Abstract Mars is typically viewed as a member of the category of weakly magnetized planets, with a largely induced magnetosphere and magnetotail produced by the draped fields of the solar wind interaction. However, selected Mars Atmosphere and Volatile EvolutioN Mission (MAVEN) suprathermal electron and magnetic field observations in the near wake, sampled along its elliptical orbit during the early prime mission at altitudes ranging from its ~150 km periapsis to the tail magnetosheath, reinforce a picture seen in an MHD model where magnetic fields are rooted in the planet throughout much of the Martian magnetotail.

1. Introduction

Early observations of the Mars-solar wind interaction on the Mars 2, 3, and 5, and Phobos-2 spacecraft revealed a Mars-solar wind interaction that in many ways resembles the Venus-solar wind interaction [*Vaisberg*, 1992]. In particular, a dayside magnetic barrier composed of piled-up interplanetary field was observed by Phobos-2 during its initial transfer orbits [*Riedler et al.,* 1992], and in its final, equatorial circular orbit at ~2.75 R_{Mars}, induced magnetotail lobes like those at Venus were regularly observed [*Yeroshenko et al.,* 1990]. A hint of some difference in the Mars interaction was the apparently greater width of the Martian magnetotail boundary where solar wind fluxes were no longer observed in the wake [e.g., *Luhmann et al.,* 1991; *Zhang et al.,* 1994]. Nevertheless, the larger-scale height of the Martian atmosphere/ionosphere relative to the planet radius, its weaker ionosphere and weaker incident solar wind at Mars' heliocentric distance, and the likely role of ion kinetic effects on the plasma interaction at Mars made this difference unsurprising.

In 1998 The Mars Global Surveyor (MGS) detected the crustal remanant magnetic fields of Mars, forever changing our view of this planet and its solar wind interaction [*Acuna et al.,* 2001]. The related details were subsequently investigated to the extent the MGS transfer orbits and polar mapping orbit at ~400 km fixed 2 A.M.–2 P.M. local time allowed [e.g., *Brain et al.,* 2006]. Combined analyses of the Electron Reflectometer and the magnetometer data [*Mitchell et al.,* 2001] provided information on attributes unique to the Mars obstacle, including the spatial mapping of local magnetic fields that originated from (1) draped magnetosheath fields, (2) field loops rooted in the planet (closed fields), and (3) fields with one end rooted in the planet and at the other end extending into interplanetary space (open fields). Some consequences of this topology included a complex topside ionospheric topology [*Mitchell et al.,* 2001], signatures of magnetic reconnection between external and crustal fields at the solar wind boundary including flux ropes or plasmoids [*Brain et al.,* 2010], and crustal field-associated aurora [*Brain et al.,* 2006]. The Mars Express mission has been subsequently orbiting Mars in a highly elliptical orbit with an ionosphere-probing radar and plasma ion composition and electron spectrometers, obtaining much new information on the structure and composition of the ionosphere and the planetary ions in the wake [*Lundin and Barabash*, 2004; *Fedorov et al.,* 2008]. However, its lack of a magnetometer limits interpretation of the observed features and phenomena.

The general properties of induced magnetospheres of weakly magnetized planets are well known from missions to Venus [e.g., *Luhmann*, 1986; *Luhmann et al.,* 2004; *Bertucci et al.,* 2011]. Magnetic fields in the wakes of such obstacles are generally connected to the interplanetary field, having acquired a comet-like

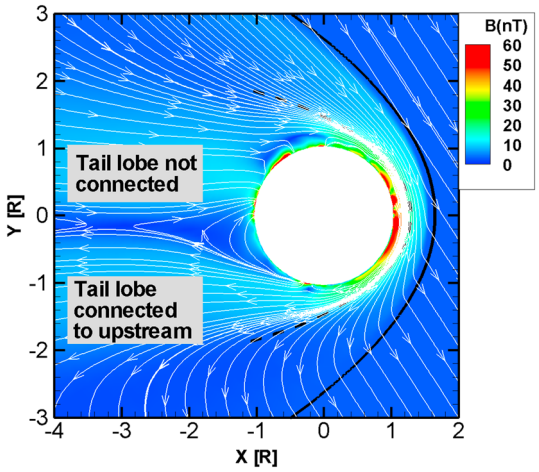

Figure 1. Magnetic field lines in the equatorial plane obtained from an MHD simulation of the Mars-solar wind interaction, assuming nominal solar wind properties and a Parker Spiral interplanetary field. In this case, the strong crustal fields are at noon. The connectivity of the magnetotail lobes to the external field is indicated. Instead of draped interplanetary fields, the model shows most wake fields connected to Mars.

draped field configuration from the planetary atmosphere/ionosphere interaction. These induced magnetotails are produced by solar wind stagnation and diversion around the ionosphere, combined with mass loading by planetary ion production on the draped fields—some of which penetrate into the main ionosphere. However, at Mars, where the planetary crustal fields provide a significant part of the obstacle pressure that counters the incident solar wind pressure [e.g., *Ma et al.,* 2004], both collisionless and collisional reconnections between external and crustal fields produce a wake that contains combinations of open, closed, and draped field topologies [*Ferguson et al.,* 2005; *Halekas et al.,* 2006, 2009].

Since its orbit insertion in November 2014, MAVEN has made observations around Mars with a full complement of particle and field instruments [*Jakosky et al.,* 2015a]. The early prime mission provided many measurements in the solar wind wake from ionospheric altitudes at its ~150 km periapsis to several Mars radii, including plasma ions and electrons and magnetic fields [*Connerney et al.,* 2015]. At the same time, solar wind interaction models have been run toward improving our ability to understand the global context of the measurements, while validating the model results. The present study uses a small portion of these combined observations and models to learn more about the nature of the Mars obstacle to the solar wind and, in particular, whether a more magnetospheric than ionospheric solar wind obstacle picture, suggested by the models, currently applies.

2. Approach

Even before Mars Atmosphere and Volatile EvolutioN Mission (MAVEN) arrived at Mars, it was realized that the Mars-solar wind interaction is complicated and dynamic on many time and spatial scales due to the combination of varying solar and solar wind parameters, an atmosphere/ionosphere that responds to both external and planetary influences, and high harmonic order, geographically nonuniform, crustal magnetic fields that rotate with the planet [e.g., *Brain et al.,* 2003]. Many open questions remain that impact efforts to understand its global and evolutionary consequences. In particular, the role of a planetary magnetic field in shielding an atmosphere from solar wind erosion over time continues to be debated [e.g., *Moore and Horwitz*, 2007].

From the first acquisitions of the MAVEN plasma and field data, BATS-R-US MHD simulations of the solar wind interaction [*Ma et al.,* 2004, 2014] have been compared with observations along the orbit with sometimes remarkable agreement for even single-fluid, multispecies models [e.g., *Jakosky et al.,* 2015a]. The comparisons generally include the vector magnetic field measurements, the solar wind plasma ion densities and velocities, and the upper ionosphere ion composition measurements (see *Jakosky et al.* [2015b]). A major goal of these model fittings has been to infer the related global ionospheric escape rates for realistic solar wind interaction geometries. However, they also lend themselves to investigating the topology and origins of fields making up the Mars obstacle.

Figure 1 shows some equatorial field lines from one of the MHD simulations for typical solar wind conditions and a Parker Spiral interplanetary field. Here all the expected wake field topologies are present. What is particularly notable, however, is the existence of a large volume of the wake that is occupied by fields rooted in Mars, including both closed loops and the premidnight (upper) tail lobe. While this is a model result, it raises the interesting question of whether this topology exists at Mars.

Dubinin et al. [1994] applied Phobos-2 solar wind electron streaming and magnetometer observations to investigate the topology of the Martian magnetotail at ~2.8 R_{Mars}. Based on the observed streaming anisotropies (these electrons stream outward from the Sun along the interplanetary field), they concluded that the magnetotail appeared induced, like the Venus tail. Later analyses using data from the MGS magnetometer and Electron Reflectometer examined the open/closed/draped nature of the field in the Mars wake at ~400 km altitude along that spacecraft's 2 A.M.–2 P.M. polar orbit [*Mitchell et al.,* 2001; *Brain*, 2006]. The connection between the low- and high-altitude pictures was partly addressed by *Liemohn et al.* [2006] who used BATS-R-US MHD models of the Mars-solar wind interaction, with electron observations from the ELectron Spectrometer (ELS) experiment on Mars Express, to infer the dayside origins of photoelectrons observed in the Martian wake. This later work mapped model open field lines rooted in the dayside ionosphere to the location of the spacecraft and found good agreement. However, the nightside ionosphere does not provide photoelectron tracers to interpret the more global magnetospheric field topology.

With MAVEN's data sets we can use combined particle and field measurements to further investigate the connections of different regions in the wake to the solar wind or ionosphere. Here we take advantage of a period of exceptionally steady interplanetary conditions to infer the related field topologies in the near-Mars wake. The period from 19 December 2014 to 22 December 2014 had typical solar wind pressures, and a particularly steady "toward" sector (B_{ymso} negative, or westward, and Bx_{mso} positive, or Sunward, where "mso" stands for the standard Mars-centered solar orbital coordinate system) Parker Spiral interplanetary fields. The behavior of both the magnetic field and suprathermal electrons in the solar wind wake are used to confirm the pattern of field draping and magnetic connectivities, respectively. We use SWEA (Solar Wind Electron Analyzer) key parameters to characterize the anisotropy of the local suprathermal electrons with respect to the wake magnetic fields, and the magnetometer to determine the local field orientation. Together, these can tell us whether MAVEN is connected to the solar wind only (draped field), the ionosphere only (closed field), or both (open field).

For global perspective, BATS-R-US MHD simulations were run for a Westward Parker Spiral external field orientation and a variety of crustal field orientations to determine the expected Martian wake field topologies for these conditions. The details of the basic simulations are described in earlier references and are not repeated here. The main points of interest for this study are the spatial resolution, which is ~5–10 km in the ionosphere, the assumption than the *Arkani-Hamed* [2002] crustal field model is specified at the inner boundary at ~100 km, and the influence of numerical diffusion in controlling where magnetic reconnection occurs in most of the simulation space. As the latter determines the magnetic field topologies in the simulation, consistencies between observations and models are often used as an implicit measure of its goodness as an approximation. We traced model magnetic field lines from a spherical grid of starting points at 150 km altitude (below the nominal exobase of Mars) to determine whether they were connected to the lower boundary at both ends (closed), connected to the lower boundary at one end and passing through a Mars-centered, 3 R_{Mars} surface at the other (open), or passing through the 3 R_{Mars} surface at both ends (draped). One general result of note is how magnetically closed much of the 150 km altitude surface often is according to the models. Another is that large portions of the magnetotail cross section from low wake altitudes to several Mars radius distances are found to be open fields connected to the inner simulation boundary, rather than draped, as one would find in a strictly induced magnetotail.

3. Analysis

Figure 2 displays model cross-tail field topologies obtained at $X_{mso} = -1.1\ R_{Mars}$ in the wake, determined by the model field line tracings starting from 150 km altitude mentioned above. For this study we show Westward Parker Spiral field results only, with the strongest crustal fields located at noon, dusk, midnight, and dawn under equinox conditions. The different shadings and colors identify both field topology type (open, closed, or draped), as well as polarity (outward (+) or inward (−) with respect to Mars). The cross sections show a marked contrast to the usual induced magnetosphere picture where an approximately north-south tail polarity boundary or current sheet, separating two positive and negative draped field lobes, is expected. Of particular interest here are the large areas of open, rather than draped, fields, extending well outside the optical shadow indicated by the black line. These large areas occupy space that is roughly equal to the Mars magnetic tail boundary cross section inferred from observations (see *Jakosky et al.* [2015b]). Moreover, while the

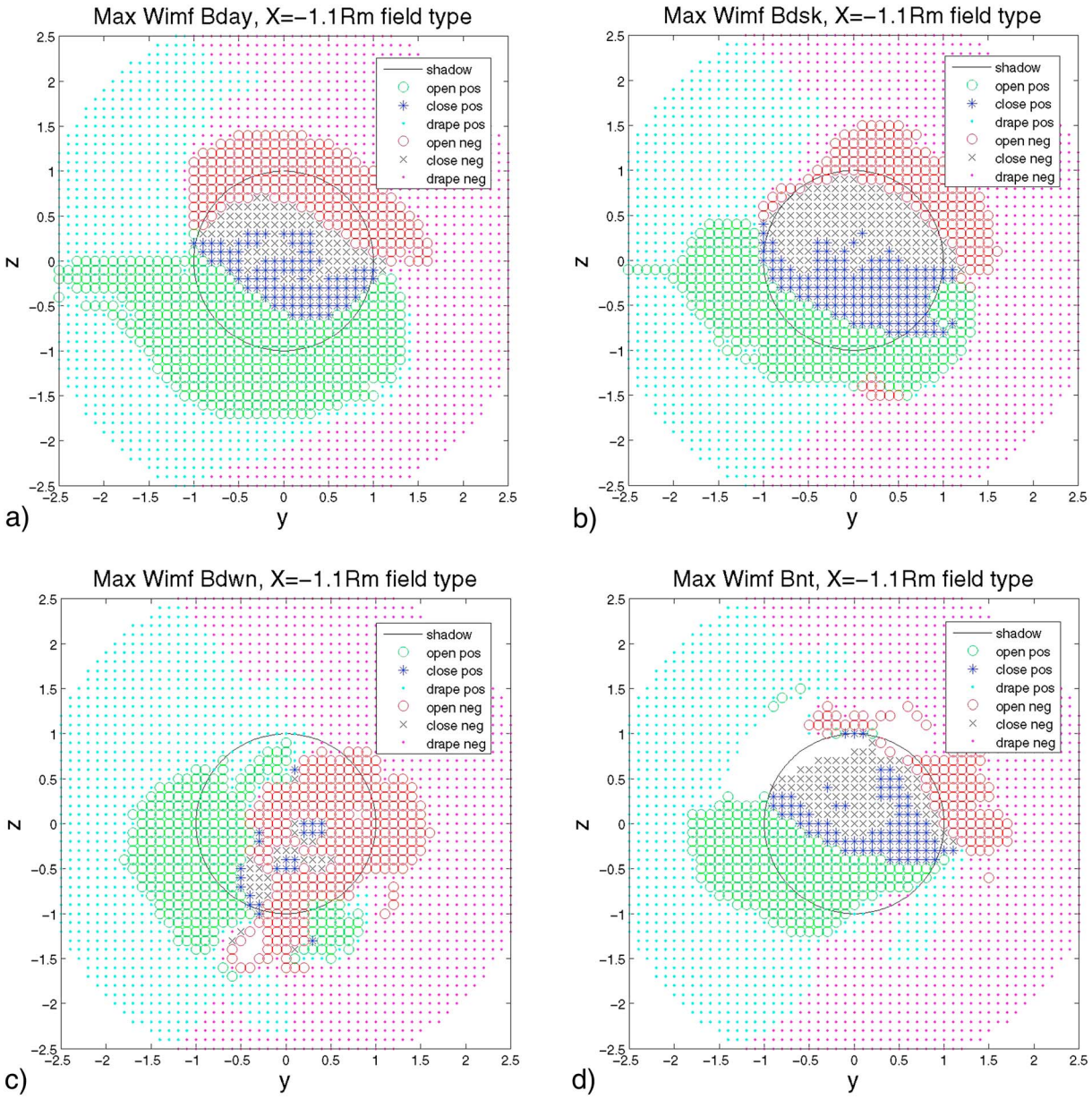

Figure 2. Cross sections of the wake from MHD simulations of the Mars-solar wind interaction for Westward Parker Spiral interplanetary field and the strong crustal fields located at (a) noon, (b) dusk, (c) dawn, and (d) midnight, showing areas of different magnetic field topologies: draped, closed and open, and polarities: outward (+) or inward (−). The view is from the Sun. The black circles in the center indicate the optical shadow. Notice that the dawn crustal field case has the polarity pattern of a purely induced tail, with a north-south current sheet, but the central wake is dominated by "open" fields connected to the planet.

outermost, draped portion of the fields are generally consistent with an eastward/westward separation of tail lobe polarity, the open field areas interior to these often show a more north-south polarity division. Interestingly, one of these crustal field orientations (e.g., dawn, Figure 2, lower left) maintains an almost induced tail field polarity pattern at the downtail distance shown, with the distinction that the lobes are not induced in the traditional sense of the word because they contain large areas of fields connected to the planet. The model results for at $X_{mso} = -2.0\, R_{Mars}$ look similar but with a decreased contribution of closed fields.

The data analysis was designed to test whether a substantial portion of the observed tail lobes are rooted to the planet rather than draped, as the models suggest. We use a variant of the method used by *Dubinin et al.* [1994] on Phobos-2 data, described earlier. The method takes advantage of the fact that suprathermal solar electrons (energies > ~50 eV) stream away from their source in the solar corona and are ubiquitously present

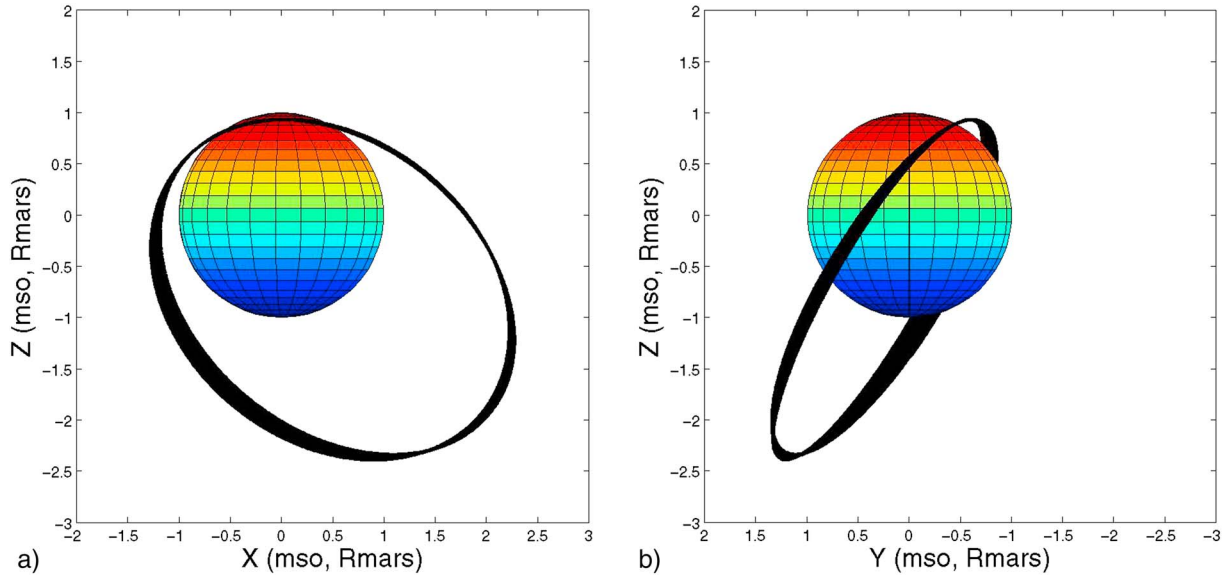

Figure 3. MAVEN orbits for 19–22 December 2014 in the MSO system. (a) The meridian view (Sun is at +*x*). (b) Looking from the wake back toward the Sun. These orbits sampled the low-altitude wake.

in the solar wind in the inner heliosphere. Induced tail lobes should thus show a suprathermal electron flux anisotropy that is everywhere parallel or antiparallel to the field, depending on whether the interplanetary field sector is respectively eastward/away or westward/toward. An induced magnetotail should show a simple reversal of the solar electron streaming when the draped (in that case) tail lobe fields reverse direction. However, if a tail lobe is rooted in the planet, as suggested in Figure 1, it is not magnetically connected to the Sun and should be depleted of these electrons. . Even if some solar wind electrons migrate across magnetic field lines in the Mars wake, due to wave-related scattering or drifts for example, the external anisotropy should be absent. Thus, for a westward Parker Spiral interplanetary field the negative B_{xmso} tail lobe should exhibit the upstream/sheath suprathermal electron streaming, while the positive B_{xmso} tail lobe should not.

MAVEN's SWEA observes electrons in the few eV to 1 keV energy range over a nearly 4 pi field of view [*Jakosky et al.*, 2015b]. SWEA and magnetometer Key Parameters are produced as a part of the regular archived MAVEN data sets. These 8 s averages are time-synchronized so they can be easily used for comparisons of diverse quantities. Here we focus on the SWEA Key Parameters that describe parallel and antiparallel (to the local magnetic field) fluxes of electrons in the energy range 100 eV to 500 eV. These are safely within the range where the solar wind suprathermal electron streaming is observed [e.g., *Lin*, 1998] while including sufficiently high fluxes for accurate measurements unaffected by spacecraft potentials. We examine both the relative and absolute fluxes for both the region within the optical shadow (see Figure 2) and outside. These are compared to the local magnetic field polarities (signs of the sunward-antisunward or B_{xmso} components) in the Mars wake.

By using the period of exceptionally steady Westward Parker Spiral field in December 2014 mentioned above, this study minimizes ambiguities from time-dependent interplanetary fields, allowing us to look for persistent patterns of behavior. The orbits for the period 19–22 December 2014 are very similar as shown in Figure 3 where they are overlaid. For this period MAVEN periapsis is in the nightside, providing a wake field sample of ~15 orbits that cross through structure like that in Figure 1 in the low-altitude tail and adjacent magnetosheath. Mars rotates under the orbit so that the crustal field effects on the wake change, nominally introducing some variations in the wake field topology such as those illustrated in Figure 2.

General attributes of the suprathermal electron field-aligned net fluxes are illustrated in Figure 4a, where they are plotted against distance (rho) from the center of the optical wake axis. In this plot and subsequent plots, par2 is the Key Parameter describing the 100–500 eV electron flux integrated over the SWEA field of view hemisphere centered on the average field direction (parallel flux), and antipar2 (also referred to as anti2 in the plots) is the corresponding quantity for the opposite hemisphere—the antiparallel flux. The display in

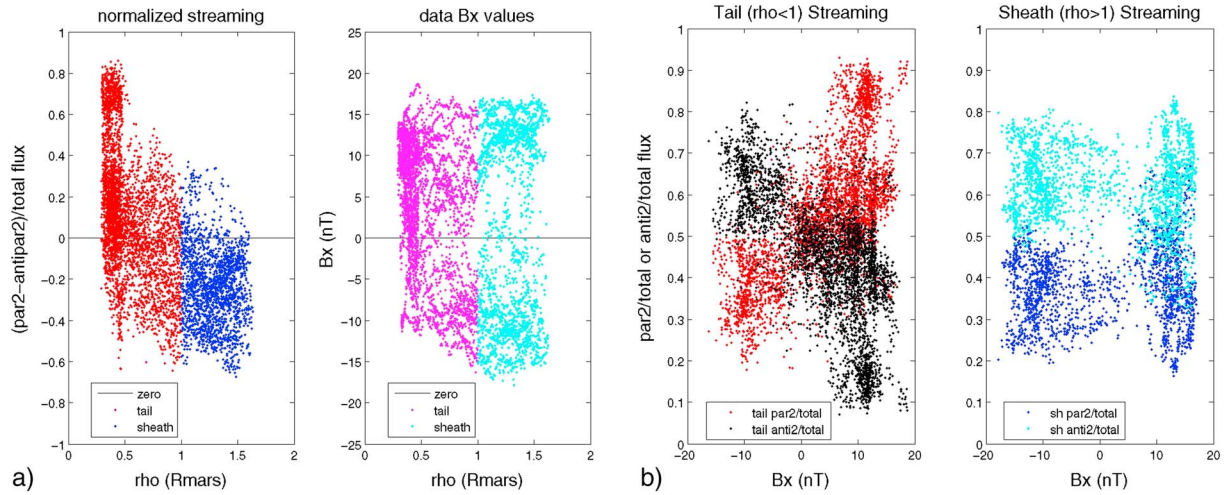

Figure 4. (a) Plots showing the distribution of the data sample parallel (par2) and antiparallel (antipar2) 100–500 eV electron flux relative streaming, normalized by the total flux (Figure 4a (left)) for tail (rho $< 1\ R_{Mars}$) and sheath (rho $> 1\ R_{Mars}$) spatial samplings at $X_{mso} < 1\ R_{Mars}$. The solar/antisolar (B_{xmso}) components of the magnetic field for these samples are shown in Figure 4a (right). Notice that antiparallel streaming prevails in the sheath (and upstream) while streaming is mixed in the tail. (b) Plot showing MAVEN SWEA Key Parameter (8 s average) suprathermal electron flux anisotropies at 100–500 eV energies, where parallel and antiparallel fluxes are normalized by the total fluxes. Figure 4b (left) is for the data obtained in the optical shadow (within 1 R_{Mars} of the $-X_{mso}$ axis), while Figure 4b (right) is from the surrounding area sampled along the orbit paths in Figure 3.

Figure 4a (left) uses the difference between these fluxes, normalized by their sum, to provide and overall sense of streaming directions in the low-altitude wake. The "sheath" portion (rho $> 1\ R_{Mars}$) exhibits the overall negative values representing the antiparallel streaming expected for the prevailing draped interplanetary field. In contrast, the "tail" portion (rho $< 1\ R_{Mars}$) is mixed, with samples showing both net streaming directions and also possible counter streaming (small values of the difference). Figure 4a (right) displays the magnetic field B_{xmso} components for this data set, where both polarities are seen in both spatial domains. Various combinations of these data were used to explore the topological questions described above, a subset of which we show here.

Figure 4b shows the correlations found between 100 and 500 eV electron streaming and the sign of B_{xmso} for both the central tail defined here by the optical shadow region and the surrounding draped/sheath regions —both tailward of $X_{mso} = -1\ R_{Mars}$. Here we normalize the parallel and antiparallel fluxes by the combined flux to bring out the electron streaming patterns regardless of flux magnitudes. The draped/sheath region results in Figure 4b (right) again show the clear dominance of the antiparallel flux (antipar2) expected for the prevailing toward Parker Spiral interplanetary field—regardless of whether the draped field "lobe" is $+B_{xmso}$ or $-B_{xmso}$. However, in the analogous central wake observations plotted on the left, a clear reversal of streaming behavior is seen when the sign of the field reverses. While the $-B_{xmso}$ lobe results on Figure 4b (left) of this plot closely resemble the induced/draped field results in Figure 4b (right), as expected (see Figure 1), the $+B_{xmso}$ lobe shows both the opposite streaming direction and a greater spread of flux values.

The field geometry in Figure 1 suggests that another indication of its validity should be a relative lack of antiparallel solar electron streaming in the unconnected ($+Y$ or $+B_{xmso}$) tail lobe compared to the Sun-connected ($-Y$, or $-B_{xmso}$) tail lobe. We analyzed the $+B_{xmso}$ and $-B_{xmso}$ tail and sheath region parallel to antiparallel electron flux ratios to compare their average values. The tail ratios should be larger in the tail lobe that is disconnected from the solar source, while in the Sun-connected tail lobe they should be comparable to the sheath ratios. As expected for draped fields, the sheath parallel-to-antiparallel flux ratios are similar for both tail lobes at 0.71 for the $+B_{xmso}$ lobe and 0.60 for the $-B_{xmso}$ lobe. The statistical errors in these ratios are less than a percent. For the tail region, the $-B_{xmso}$ (Sun-connected) lobe has a similar ratio of 0.74, but the $+B_{xmso}$ lobe has a ratio of 2.22. Analysis of the average fluxes involved in these ratios shows that the latter is due to a relatively low-average antiparallel flux, which would be expected for loss of the direct solar connection of this tail lobe. . Our interpretation is that the $+B_{xmso}$ tail lobe is emptier of suprathermal electrons than the $-B_{xmso}$

tail lobe, although it still provides an access path for sunward moving electrons to reach the nightside ionosphere. This is consistent with expectations for a wake field topology like that in Figure 1.

4. Conclusions

For weakly magnetized planets like Mars and Venus, an often standard assumption is that the magnetotail is a primarily induced structure composed of effectively draped interplanetary magnetic fields. However, the models of the Mars-solar wind interaction imply that there are considerable differences from this picture at Mars, even though the crustal remanent fields are nonuniform and composed of mainly high-order spherical harmonic contributions that fall off rapidly with radial distance. In particular, magnetic fields rooted in the planet may fill a significant volume of the near wake. Here observations of selected suprathermal electron streaming data in the Mars wake obtained with the combined MAVEN SWEA and magnetometer data are used to investigate consistency with these model results. The inference is that a double-lobe, draped interplanetary field, induced tail structure may be rarely realized, at least at the present epoch, and that previous observations of what appeared to be an induced magnetotail contain more planetary fields than were initially assumed. The MAVEN data analyzed here support this picture. They show that suprathermal electron streaming seen in the solar wind fills the Mars magnetotail lobe that is directly connected to interplanetary space, while this streaming flux is largely absent and, in fact, in the opposite direction, on the lobe that originates at the planet. Thus, Mars is in some ways a more Moon-like than Venus-like obstacle. These results also have implications for the reported solar electron event-related auroras [*Jakosky et al.*, 2015b] as well as for reconnection geometries and their consequences [e.g., *Brain et al.,* 2006; *Halekas and Brain*, 2009], both of which are affected by the magnetic topology of the Martian obstacle.

Finally, the results suggest caution in organizing all observed features and phenomena in a manner that assumes a classically induced magnetosphere picture. While the solar wind and draped magnetosheath magnetic field and dayside planetary ion production may dominate the geometry of the observed escaping pickup ion plumes and related dayside precipitation [*Fang et al.,* 2010], the interpretation of other planetary ions and magnetic structure (and processes) in the solar wind wake is a greater challenge. Indeed, the strengths of the atmosphere and solar EUV fluxes are important factors in determining whether a weakly magnetized planet interaction is primarily induced or not. The Mars solar wind obstacle may, in fact, morph from one state to another depending on the circumstances. For example, a largely induced magnetotail may have resulted when solar EUV fluxes were much higher than at present during the maximum of solar cycle 22 when the Phobos-2 measurements were obtained. The possibility that the wake fields are draped fields that simply pass through the collisional atmosphere where the solar wind electrons are removed cannot be discounted. While the models fix the inner boundary field to the MGS map, even the origin of those fields is not well understood [e.g., *Luhmann et al.,* 2015]. Further investigations of the present Mars obstacle magnetic topology will be possible as greater spatial and temporal sampling is obtained as the MAVEN mission proceeds.

Acknowledgments
The MAVEN mission, led by coauthor and Principal Investigator Bruce M. Jakosky, is supported by NASA through its Mars Exploration Program. We are grateful to the spacecraft builders at Lockheed-Martin in Littleton, CO, the Project Leaders and Managers at Goddard Space Flight Center and NASA, the Science Operations Center at Laboratory for Space Physics, University of Colorado, Boulder, and the instrument providers who worked tirelessly to realize the MAVEN data. The data used here are part of the MAVEN archive accessible through NASA's Planetary Data System. This work was enabled through partial support of SWEA by CNES.

References

Acuna, M., et al. (2001), The magnetic field of Mars: Summary of results from the aerobraking and mapping orbits, *J. Geophys. Res.*, *106*, 23,403–23,417, doi:10.1029/2000JE001404.

Arkani-Hamed, J. (2002), An improved 50-degree spherical harmonic model of the magnetic field of Mars derived from both high altitude and low altitude data, *J. Geophys. Res.*, *107*, doi:10.1029/2001JE001835.

Bertucci, C., F. Duru, N. Edberg, M. Fraenz, C. Martinecz, K. Szego, and O. Vaisberg (2011), The induced magnetosphere of Mars, Venus and Titan, *Space Sci. Rev.*, *162*, 113–171.

Brain, D. A. (2006), Mars Global Surveyor measurements of the Martian plasma interaction, *Space Sci. Rev.*, *126*, 77–112.

Brain, D. A., F. Bagenal, M. H. Acuna, and J. E. P. Connerney (2003), Martian magnetic morphology: Contributions from the solar wind and crust, *J. Geophys. Res.*, *108*, 1424, doi:10.1029/2002JA009482.

Brain, D. A., J. S. Halekas, L. M. Peticolas, R. P. Lin, J. G. Luhmann, D. L. Mitchell, G. T. Delory, S. W. Bougher, M. H. Acuna, and H. Reme (2006), On the origin of aurorae on Mars, *Geophys. Res. Lett.*, *33*, L01201, doi:10.1029/2005GL024782.

Brain, D. A., A. H. Baker, J. Briggs, J. P. Eastwood, J. S. Halekas, and T.-D. Phan (2010), Episodic detachment of Martian crustal magnetic fields leading to bulk atmospheric plasma escape, *Geophys. Res. Lett.*, *37*, L14108, doi:10.1029/2010GL043916.

Connerney, J. E. P., J. Espley, P. Lawton, S. Murphy, J. Odom, R. Oliverson, and D. Sheppard (2015), The MAVEN magnetic field investigation, *Space Sci. Rev.*, doi:10.1007/s11214-015-0169-4.

Dubinin, E., R. Lundin, and K. Schwingenschuh (1994), Solar wind electrons as tracers of the Martian magnetotail topology, *J. Geophys. Res.*, *99*, 21,223–21,240, doi:10.1029/94JA01271.

Fang, X., M. W. Liemohn, A. F. Nagy, J. G. Luhmann, and Y. Ma (2010), Escape probability of Martian atmospheric ions: Controlling effects of the electromagnetic fields, *J. Geophys. Res.*, *115*, A04308, doi:10.1029/2009JA014929.

Fedorov, A., et al. (2008), Comparative analysis of Venus and Mars magnetotails, *Planet. Space Sci.*, *56*, 812–817.
Ferguson, B. B., J. C. Cain, D. H. Crider, D. A. Brain, and E. M. Harnett (2005), External fields on the nightside of Mars at Mars Global Surveyor mapping altitudes, *Geophys. Res. Lett.*, *32*, L16105, doi:10.1029/2004GL021964.
Halekas, J. S., and D. A. Brain (2009), Global distribution, structure, and solar wind control of low altitude current sheets at Mars, *Icarus*, doi:10.1016/j.icarus.2008.12.032.
Halekas, J. S., D. A. Brain, R. J. Lillis, M. O. Fillinghim, D. L. Mitchell, and R. P. Lin (2006), Current sheets at low altitudes in the Martian magnetotail, *Geophys. Res. Lett.*, *33*, L13101, doi:10.1029/2006GL026229.
Jakosky, B. M., et al. (2015a), The MAVEN mission to Mars, *Space Sci. Rev.*, doi:10.1007/s11214-015-0139-x.
Jakosky, B. M., et al. (2015b), MAVEN observations of the response of Mars to an interplanetary coronal mass ejection, *Science*, doi:10.1126/science.aad0210.
Liemohn, M. W., Y. Ma, R. A. Frahm, X. Fang, J. U. Kozyra, A. F. Nagy, J. D. Winningham, J. R. Sharber, S. Barabash, and R. Lundin (2006), Mars global MHD predictions of magnetic connectivity between the dayside ionosphere and the magnetospheric flanks, *Space Sci. Rev.*, *63–76*.
Lin, R. P. (1998), WIND observations of suprathermal electrons in the interplanetary medium, *Space Sci. Rev.*, *86*, 61–78.
Luhmann, J. G. (1986), The solar wind interaction with Venus, *Space Sci. Rev.*, *44*, 241–306.
Luhmann, J. G., C. T. Russell, K. Schwingenschuh, and Y. Yeroshenko (1991), A comparison of induced magnetotails of planetary bodies: Venus, Mars and Titan, *J. Geophys. Res.*, *96*, 11,199–11,208, doi:10.1029/91JA00086.
Luhmann, J. G., S. A. Ledvina, and C. T. Russell (2004), Induced magnetospheres, *Adv. Space Res.*, *33*, 1905–1912.
Luhmann, J. G., Y. J. Ma, D. A. Brain, D. Ulusen, R. J. Lillis, J. S. Halekas, and J. R. Espley (2015), Solar wind interaction effects on the magnetic fields around Mars: Consequences for interplanetary and crustal field measurements, *Planet. Space Sci.*, *117*, 15–23.
Lundin, R., and S. Barabash (2004), The wakes and magnetotails of Mars and Venus, *Adv. Space Res.*, *33*, 1945–1955.
Ma, Y., A. F. Nagy, I. V. Sokolov, and K. C. Hansen (2004), Three-dimensional, multispecies, high spatial resolution MHD studies of the solar wind interaction with Mars, *J. Geophys. Res.*, *109*, A07211, doi:10.1029/2003JA010367.
Ma, Y., X. Fang, C. T. Russell, A. F. Nagy, G. Toth, J. G. Luhmann, D. A. Brain, and C. Dong (2014), Effects of crustal field rotation on the solar wind plasma interaction with Mars, *Geophys. Res. Lett.*, *41*, 6563–6569, doi:10.1002/2014GL060785.
Mitchell, D. L., R. P. Lin, C. Mazelle, H. Rème, P. A. Cloutier, J. E. P. Connerney, M. H. Acuña, and N. F. Ness (2001), Probing Mars' crustal magnetic field and ionosphere with the MGS Electron Reflectometer, *J. Geophys. Res.*, *106*, 23,419–23,428, doi:10.1029/2000JE001435.
Moore, T. E., and J. L. Horwitz (2007), Stellar ablation of planetary atmospheres, *Rev. Geophys.*, *45*, RG3002, doi:10.1029/2005RG000194.
Riedler, W., K. Schwingenschuh, H. Lichtenegger, D. Mohlmann, J. Rustenbach, Y. Yeroshenko, J. Achache, J. Slavin, J. G. Luhmann, and C. T. Russell (1992), Interaction of the solar wind with the planet Mars: Phobos 2 magnetic field observations, *Planet. Space Sci.*, *39*, 75–81.
Vaisberg, O. L. (1992), The solar wind interaction with Mars: A review of results from early Soviet missions to Mar s, in *Venus and Mars: Atmospheres, Ionospheres and Solar Wind Interactions*, vol. 66, pp. 311–326, AGU Monograph, Washington, D. C.
Yeroshenko, Y., W. Riedler, K. Schwingenschuh, J. G. Luhmann, M. Ong, and C. T. Russell (1990), The magnetotail of Mars: Phobos observation, *Geophys. Res. Lett.*, *17*, 885–888, doi:10.1029/GL017i006p00885.
Zhang, T.-L., K. Schwingenschuh, C. T. Russell, J. G. Luhmann, H. Rosenbauer, M. I. Verigin, and G. Kotova (1994), The flaring of the Martian magnetotail observed by the Phobos 2 spacecraft, *Geophys. Res. Lett.*, *21*, 1121–4, doi:10.1029/94GL01073.